Harmonic and Transient Magnetic analysis of Single Turn Coils fed by a Current Pulse at Low and Medium Frequency

O. MALOBERTI*[1], O. MANSOURI[1], D. JOUAFFRE[2], D. HAYE[2], J. DEROSIERE[3], G. LEMBROUCK[3]
[1]ESIEE Amiens, [2]PFT Innovaltech, [3]BASIS Power Electronics
*Corresponding author: 14 quai de la Somme 80080 Amiens cedex, France (maloberti@esiee-amiens.fr)

Abstract: This paper proposes to compute the electromagnetic behavior of a single turn toroidal coil fed by a transient current at low or medium frequency thanks to both harmonic and transient finite element analysis. The aim of this study is to evaluate the accuracy and reliability of a 2D axi-symmetrical numerical model by comparing with 3D reference calculations in order to build an approximate but reliable solution that might ease either the transient calculation or the coupling with electrical, mechanical and thermal physics. After an introduction part 1, the part 2 gives the model geometry, physics and meshing. Magneto-harmonic and transient computations are carried out, shown and discussed in parts 3 and 4, before finally concluding in part 5.

Keywords: Harmonic and Transient, Magnetic Field, Magnetic Vector Potential, Single Turn Coil, Low Frequencies, Eddy Currents, Skin Effect, Lorentz Force, Equivalent Resistance and Inductance, Energy Balance.

1. Introduction

Single turn coils are used in pulsed magnetic technologies [1-7] for which both magneto-harmonic and transient magnetic analysis are required. We suggest studying one single turn coil example made of a conducting massive coil, an optional conducting field shaper and an internal conducting tube supposed to be deformed. Due to a cut within the toroidal coil between the two terminals, it is rigorously a 3D component with no axial symmetry. Because this cut is very small, we would like to investigate the possibility to reduce this geometry into an equivalent 2D axi-symmetrical model, giving with a very good approximation the true magnetic field and current density. Since the coil is highly conducting and the source is varying very quickly in time (from 10 to 100 kHz), we suggest computing the model for both harmonic and transient states in order to analyze the eddy currents, skin effects and induced Lorentz forces.

2. 3D model and 2D approximation

We propose to analyze a 3D toroidal single turn coil with a cut and feeding terminals. Due to two symmetries ((x,y) is a π+ symmetry plane and (y,z) is a π- symmetry plane), the problem can be reduced to ¼ but stays three dimensional (see **Figure 1**). From now we will assume that the cut thickness is small enough to admit an axi-symmetry around the (oz) axis. By using the cylindrical coordinates (r,θ,z), this means an invariability *versus* the coordinate θ. The model reduction will have to be compared to the 3D exact solution. Depending on the reliability, it will then be possible to investigate an equivalent 2D analytical solution. The geometry proposed is defined thanks to the main following parameters: the internal R_{ci}, intermediate R_{cm} and external R_{ce} radius of the toroidal coil, and its useful L_{fi} and total L_{fe} heights (see Table 1 in the Appendix). This coil, fed by a current pulse, will generate a magnetic field pulse in the inside and so eddy currents will be induced by the resulting time varying flux inside any internal conducting part. The tube we propose to work has got a thickness e_p and the air gap between the coil and the tube is g_{pc}. There is sometimes an intermediate field shaper between the coil and the tube. This secondary coil is also a toroidal part with the same cut. Its function is to adapt a single coil to several tube radius and length by concentrating the current and the field in the useful area defined by the tube.

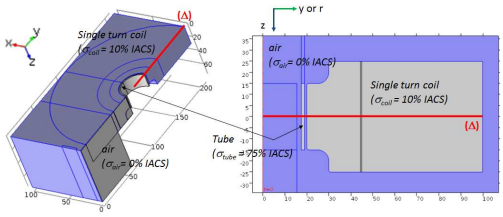

Figure 1. Geometry of the 3D geometry and its 2D reduced model.

The coil or/and field shaper are made of a steel alloy (electrical conductivity σ_c and

magnetic permeability $\mu_c=\mu_0$) and are surrounded by the air (no conductivity $\sigma_a=0$ and permeability $\mu_a=\mu_0$). The internal tube is made of a copper alloy (electrical conductivity σ_p and magnetic permeability $\mu_p=\mu_0$). (see Table 2).

We assume that neither magnetic flux nor electric current is generated outside the infinite limit (1). Due to the π^- symmetry, no magnetic flux can circulate through the (y,z) plane, and due to the π^+ symmetry, no electrical current can circulate through the (x,y) plane (1). The magnetic field **H** and flux density **B** are necessarily inside the (y,z) plane and perpendicular to the (x,y) plane. No electric current **j** can go through the air and we impose a total current $I(t)=I\exp(i\omega t)$ feeding the single coil ($\omega=2\pi f_q$ is the angle velocity and f_q the frequency) through the terminal (2). The two degrees of freedom, namely the magnetic vector potential **A** and the electric scalar potential V, linked to the magnetic and electric fields **H** and **E** respectively, are fixed to zero at initial step. All this means the following constraints at the different limits (see **Figure 2**).

$$\begin{aligned}(\infty):&\ \mathbf{n}\cdot\mathbf{B}=0\Leftrightarrow\mathbf{n}\times\mathbf{A}=\mathbf{0}\\(\pi^-):&\ \mathbf{n}\cdot\mathbf{B}=0\Leftrightarrow\mathbf{n}\times\mathbf{A}=\mathbf{0}\\(\pi^+):&\ \mathbf{n}\cdot\mathbf{j}=0\Leftrightarrow\mathbf{n}\times\mathbf{H}=\mathbf{0}\end{aligned}\qquad(1)$$

$$I=\iint_{\text{coil}}\mathbf{j}\cdot\mathbf{d}^2\mathbf{x}=\iint_{\text{coil}}(\mathbf{j}_s-\sigma\partial_t\mathbf{A})\cdot\mathbf{d}^2\mathbf{x}\qquad(2)$$

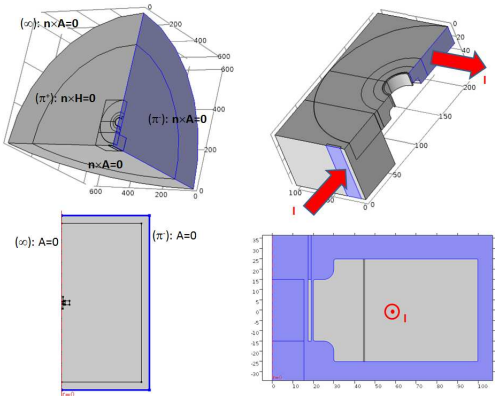

Figure 2. Constraints and Boundary conditions.

The mesh of **Figure 3** is adapted to the skin effect thanks to a skin depth parameter that depends on the permeability μ or reluctivity $\nu=\mu^{-1}$, the conductivity σ and the frequency f_q or the angular velocity $\omega=2\pi f_q$ (3). The mesh size d at the facing interfaces is chosen inferior or equal to one third of the skin depth δ.

$$\delta=\sqrt{\frac{2\nu}{\sigma\omega}}=\sqrt{\frac{\nu}{\sigma\pi fq}}\qquad(3)$$

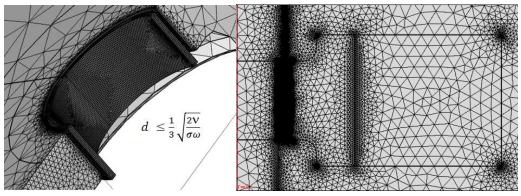

Figure 3. Meshing.

3. Magneto harmonic computations

3.1. Governing equations

The model is computed with the magnetic field formulation in the harmonic working condition first. The use of the magnetic vector potential **A** permits to automatically satisfy the magnetic flux conservation principle and the Maxwell Faraday laws. The current conservation principle and Maxwell Ampere law result in a diffusion like partial differential equation (4):

$$\nabla\times(\nu\nabla\times\mathbf{A})+j\sigma\omega\mathbf{A}=\mathbf{j}_s\qquad(4)$$

$\mathbf{j}_s$ is the current source density. σ is the electrical conductivity (σ_c = 10% IACS, σ_p = 75% IACS, σ_a = 0). ν is the magnetic reluctivity ($\nu=\mu^{-1}=\nu_0=\mu_0^{-1}(1/(4\pi)).10^7\ H^{-1}m$).

3.2. Local results

In the following we focus on local fields: the flux density **B**, the current density **j** and the Lorentz force density **f** respectively, as a function of the radial position r along the line (Δ) (5). The total current magnitude I equals 825 kA, with no phase angle and the frequency f_q= 20 kHz. All the fields can be deduced from the vector potential **A** and differential operators built with the *Nabla* operator ∇.

$$\begin{cases}\mathbf{B}=\nabla\times\mathbf{A}\\\mathbf{j}=\nabla\times(\nu\mathbf{B})=-j\sigma\omega\mathbf{A}\\\mathbf{f}=\mathbf{j}\times\mathbf{B}\end{cases}\qquad(5)$$

In **Figure 4**, **Figure 5** and **Figure 6**, we analyse some field density results as a function of the radial coordinate r along the line (Δ).

In **Figure 4**, we first observe that induction magnitude |**B**| is almost constant in the free internal space of the coil without any tube, but is rapidly decreasing inside the coil material due to the skin depth. When the tube is introduced, the skin effect remains inside both the coil and the tube materials, each with its skin depth ($\delta = \delta_1 = 1.46$ mm in the coil and $\delta = \delta_2 = 0.53$ mm in the tube). No flux is generated in the free space inside the tube such that the induction magnitude, two times higher than without the tube, is focused in the free space in between the coil and the tube.

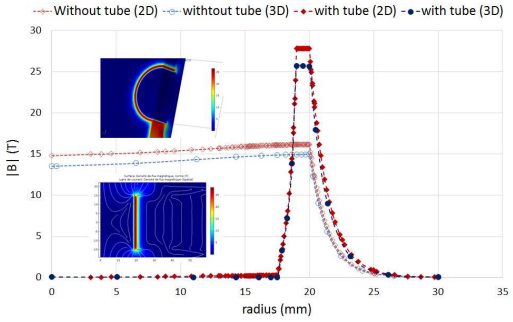

Figure 4. Magnetic flux density.

In the **Figure 5**, no current can go in the air region. The current density magnitude |**j**| is maximum at the conductors' skin and is rapidly decreasing inside both the coil and the tube skin depth. The current magnitude in the coil with the tube is two times higher than without the tube. This implies eddy currents induced in the coil with an additional phase angle. Mainly due to the higher electrical conductivity of the tube, the current density (only eddy currents) is three times higher in the tube than in the coil.

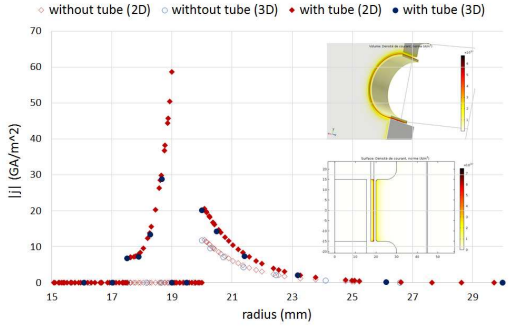

Figure 5. Electrical current density.

By using the flux density **B** and the current density **j**, we can compute the Lorentz force density **f** either by the Lorentz cross product formula (7) or the divergence of the Maxwell stress tensor **T** (6).

$$T_{ij} = \nu_0 \left(B_i B_j - \frac{1}{2} |B|^2 \delta_{ij} \right) \quad (6)$$

$$\mathbf{f} = \mathbf{j} \times \mathbf{B} = \nabla \cdot \mathbf{T} \quad (7)$$

In the **Figure 6**, no force acts on the air region. The force is always negative inside the tube, tending to compress it; and it is always positive inside the coil, tending to expand it. The force density **f**, proportional to the cross product between the current density and the flux density, behaves in magnitude inside the conducting materials similarly to the current and the induction, with a corresponding half skin depth.

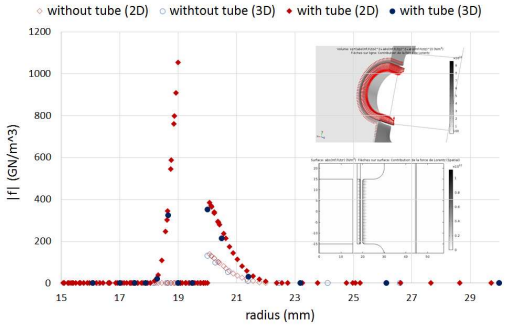

Figure 6. Lorentz force density.

Finally, we notice in **Figure 4**, **Figure 5** and **Figure 6** that an agreement is found for all the results on |**B**|, |**j**| and |**f**| between the 2D and the 3D computations with a small discrepancy which is smaller than 4% inside the conducting materials and 12% inside the air.

3.3. Global results

Now, we propose to use the electromagnetic fields, mainly the current density **j** and flux density **B**, in order to compute the main power or energy terms, such as the resistive Joule losses P_j (8) and the stored magnetic energy W_m (9).

$$P_j = \iiint_{space} \frac{|\mathbf{j}|^2}{2\sigma} d^3x \Rightarrow R = \frac{2P_j}{I^2} \quad (8)$$

$$W_m = \iiint_{space} \frac{|\mathbf{B}|^2}{2\mu} d^3x \Rightarrow L = \frac{2W_m}{I^2} \quad (9)$$

As long as the problem is linear with constant properties σ and μ, these integrals lead to the coil resistance R and inductance L [2, 3, 6].

In **Figure 7** and **Figure 8**, we draw the curves of the coil resistance and inductance as a function of the frequency with and without tube.

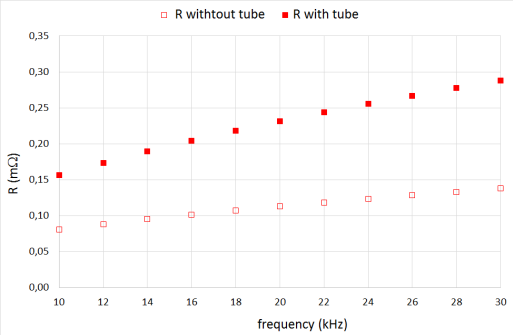

Figure 7. Equivalent coil resistance.

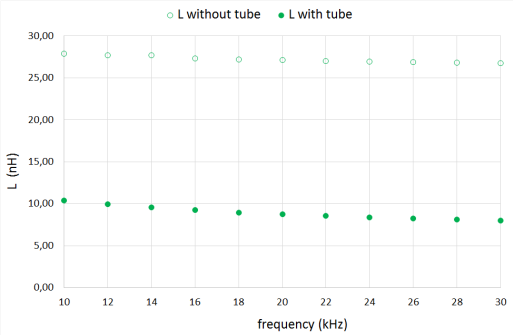

Figure 8. Equivalent coil inductance.

Finally, we can look at the maximum force density F_1 and F_2 acting on the coil (10) and the tube (11) skin respectively.

$$F_1 = \max_{coil}\{\mathbf{f}\cdot\mathbf{u}_r\} \quad (10)$$

$$F_2 = \max_{tube}\{\mathbf{f}\cdot\mathbf{u}_r\} \quad (11)$$

What is interesting is the self and mutual force density coefficients K_1 (12) and K_2 (13) respectively defined by the ratio between the maximum force density and the squared current.

$$K_1 = \frac{F_1}{I^2} = \frac{\max_{coil}\{\mathbf{f}\cdot\mathbf{u}_r\}}{I^2} \quad (12)$$

$$K_2 = \frac{F_2}{I^2} = \frac{\max_{tube}\{\mathbf{f}\cdot\mathbf{u}_r\}}{I^2} \quad (13)$$

In **Figure 9**, we draw the curves of the self and mutual force density coefficients K_1 and K_2 respectively as a function of the frequency f_q with and without the tube to deform.

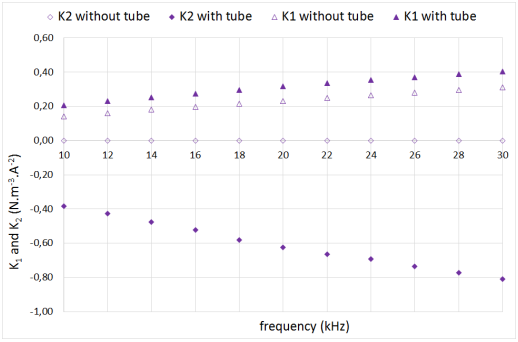

Figure 9. Equivalent force density coefficients.

3.4. Discussion on the impact of frequency

In **Figure 7**, we notice that the equivalent resistance R, approximately inversely proportional to the skin depth, increases with the frequency. This effect is of course due to the skin effect. The higher the frequency is, the thinner the skin and the bigger the resistance will be. In **Figure 8**, on the contrary, the equivalent inductance L, approximately proportional to the skin depth, decreases with the frequency. The decreasing law is smoother than for the resistance but is still due to the skin effect. These laws seem to be coherent with the decreasing law of the skin depth as a function of the frequency (3). In **Figure 9**, due to the increase of both the maximum current and flux density into the skin, the absolute force density coefficients also increase with the frequency f.

3.5. Discussion on the impact of the tube

In **Figure 7**, we notice that the equivalent resistance R is bigger with the tube than without. Two conducting regions instead of one induces automatically more eddy currents and Joule losses. In **Figure 8**, on the contrary, the equivalent inductance L is lower with the tube than without. The tube acts as a flux damper inside the free space of the entire coil. In **Figure 9**, due to local current and flux densities into the coil skin higher with the tube than without, the absolute force density coefficients are also bigger. The more conducting the material is, the higher the coefficient is and the bigger the slope of the increasing law with the frequency will be.

4. Transient Magnetic Computations

4.1. Governing equations

The model is computed with the magnetic field formulation then in the transient working condition. The Maxwell equations still result in the use of the magnetic vector potential **A** and a diffusion like partial differential equation (14). It is however necessary to add the Coulomb gauge condition (15) in this transient state in order to correctly and uniquely determine the solution.

$$\nabla\times(\nu\nabla\times\mathbf{A})+\sigma\partial_t\mathbf{A}=\mathbf{j_s} \qquad (14)$$

$$\nabla\cdot\mathbf{A}=0 \qquad (15)$$

4.2. Computation results

In **Figure 10**, we compute the absolute value of the maximum force density in the coil $|F_1|$ and in the tube $|F_2|$ as a function of time in the transient working condition.

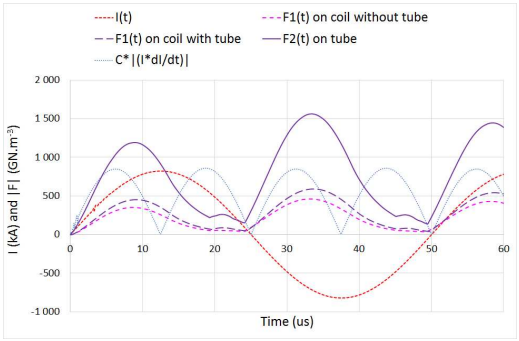

Figure 10. Maxima of the Lorentz force density.

As expected, the force is higher in the tube than in the coil and the one in the coil is higher with the tube than without the tube. The sign of each force contribution never changes and never equals zero. In fact, the internal tube can only be compressed and the external coil be expanded. It is interesting to notice that the maximum of $|F_1|$ and $|F_2|$ does not occur at the current maximum but a bit sooner. This might be due to the phase angle of eddy currents that mainly depend on the first current derivative dI/dt.

In **Figure 11**, we then compute the coil terminal voltage as a function of time still in the transient working condition and still corresponding to a sinusoidal current of magnitude I = 825 kA and frequency f_q = 20 kHz.

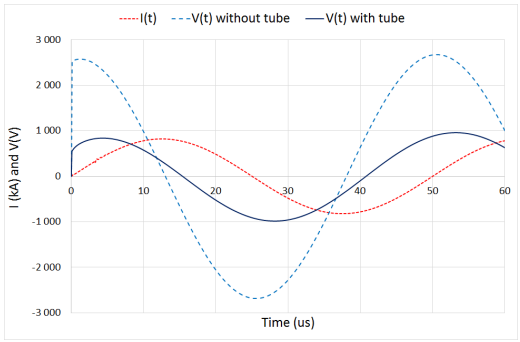

Figure 11. Transient current-voltage relationship.

At f_q = 20 kHz, the coil impedance mainly depends on the inductance part jLω. As a consequence, and accordingly to results of **Figure 8**, the coil inductance and therefore its impedance is lower with the tube than without. While constraining the total current to the same fixed value for both cases, it results in a lower computed voltage with the tube than without it. By using a voltage pulsed generator, it would result in a higher current pulse inside the coil.

4.3. Experimental results

In **Figure 12**, we compare the voltage computed and measured for another prototype. The current injected in this coil has got a decaying exponential shape with a maximum around 1 MA and a resonance frequency around 22 kHz. Agreement is found for the coil voltage computed and measured without any tube.

4.4. Discussions

Previous results are quite interesting in the system and control optimization point of view.

The mechanical parts {coil + tube} may need to control both the force density and its distribution inside the tube in order to fulfill the forming, clamping or/and welding requirements. Knowing the generator voltage V and capacity, these two can be tuned thanks to the current and its first derivative or the frequency, so thanks to the coil impedance, and mainly the inductance L.

The electrical parts {generator + coil} may need to control the power balance and the losses. These last mainly depend on the resistance R.

These two last components R and L clearly depend on the main geometrical parameters (g_{pc}, R_{ci}, L_{fi}) and material properties (σ_c, μ_c), that can therefore be sized, chosen and optimized.

5. Conclusion

In this paper we have computed the electromagnetic behavior of a single turn toroidal coil fed by a transient current at low or medium frequency thanks to both harmonic and transient finite element analysis. It has been shown that the single turn coil with a cut can be modelled thanks to an equivalent 2D axi-symmetrical model that give satisfying results close to the ones obtained with a complete 3D model. It will then be developed and coupled to the electrical circuit and mechanical deformations.

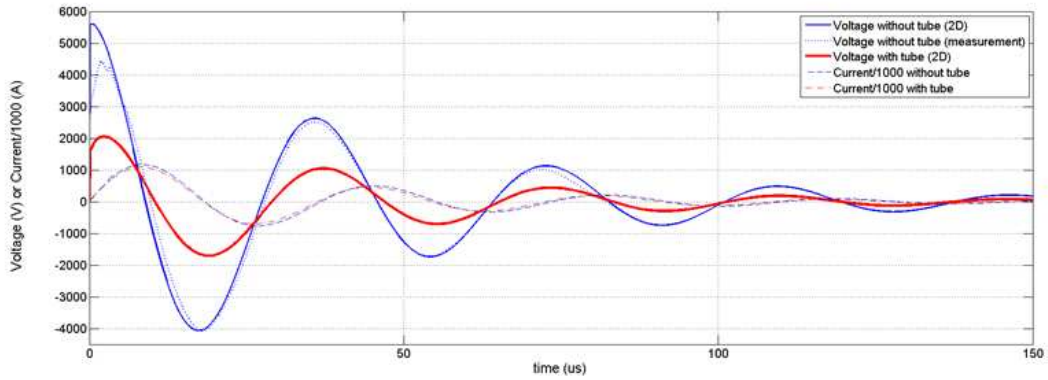

Figure 12. Comparison between computed and measured voltage on a realistic prototype.

6. References

1. G. Bartels, W. Schätzing, H.P. Scheibe, M. Leone, "Comparison of two different simulation algorithms for the electromagnetic tube compression", *Int. J. Mater. Form.*, **Vol. 2**, pages 693-696 (2009)

2. M. W. Kennedy, S. Akhtar, J. A. Bakken, R. E. Aune, "Analytical and Experimental Validation of Electromagnetic Simulations Using COMSOL®: Inductance, Induction Heating and Magnetic Fields", *Proceedings of the 2011 COMSOL Conference in Stuttgart*, (2011)

3. S. Babic, C. Akyel, "Improvement in Calculation of the Self- and Mutual Inductance of Thin Wall Solenoids and Disk Coils", *JIEEE Transactions on Magnetics*, **Vol. 36**, **n°4**, (2000)

4. R. Gersdorf, F.A. Muller, L.W. Roeland, "Design of high field magnet coils for long pulses", *JAIP Publishing, Review of Scientific Instruments*, **Vol. 36**, page 1100 (1965)

5. A. El-Azab, M. Garnich, A. Kapoor, "Modeling of the electromagnetic forming of sheet metals: state of the art and future needs", *Journal of Materials Processing Technology*, **Vol. 142**, pages 744-754 (2003)

6. H. A. Ghali, H. A. Rahman, "Understanding Mutual Inductance using Comsol® Multiphysics", *JProceedings of the COMSOL conference*, (2009)

7. K. Djellabi, M.E.H. Latreche, "Induction Heating Process Design Using Comsol® Multiphysics Software Version 4.2a", *World Academy of Science, International Journal of Electrical, Computer, Electronics and Communication*, **Vol. 8**, **n°1**, (2014)

7. Aknowledgements

We would like to express our gratitude to the Picardie Region, the Technopole and IndustriLab who gave a financial support to this work under the project called "COILTIM".

8. Appendix

Table 1: Parameters of the coil geometry.

Name	Value	significance
R_{ci}	20 mm	Internal coil radius
R_{ci}	30 mm	Intermediate coil radius
R_{ce}	100 mm	External coil radius
L_{fi}	30 mm	Internal useful length
L_{fe}	50 mm	External coil total length
ep	1.5 mm	Tube thickness
g_{pc}	1 mm	Airgap between coil and tube

Table 2: Parameters of the materials (@20°C)

Name	Value	significance
μ_0	$4\pi.10^{-7}$ H.m^{-1}	Vacuum magnetic permeability
μ_a	μ_0	Air magnetic permeability
μ_c	μ_0	Coil magnetic permeability
μ_p	μ_0	Tube magnetic permeability
σ_a	0	Air electrical conductivity
σ_c	10 % IACS*	Coil electrical conductivity
σ_p	75 % IACS*	Tube electrical conductivity
σ_{Cu}	5.8 e^{7} S.m^{-1}	Copper electrical conductivity

*IACS: International Annealed Copper Standard (100 % IACS = σ_{Cu})